Available online at www.sciencedirect.com
SCIENCE DIRECT®
Journal of Sound and Vibration 276 (2004) 27–44
JOURNAL OF SOUND AND VIBRATION
www.elsevier.com/locate/jsvi

Finite element model of a beam with a piezoceramic patch actuator

Z.K. Kusculuoglu[a], B. Fallahi[b], T.J. Royston[a,*]

[a] *Department of Mechanical Engineering, University of Illinois at Chicago, 842 West Taylor Street, Chicago, IL 60607-7022, USA*
[b] *Northern Illinois University, DeKalb, IL 60115, USA*

Received 18 November 2002; accepted 19 July 2003

Abstract

Piezoceramic wafer (patch) actuators have been used for the excitation and control of vibrations of beam and plate-like structures. Precise constitutive modelling of the system is important for accurate computer simulation. In this paper, a finite element model of a beam with a piezopatch actuator adhered to it is presented. Both the beam and the patch actuator are modelled using Timoshenko beam theory. Constraints are introduced to ensure continuity of the axial and transverse displacements at the interface of the two Timoshenko elements. This formulation allows the cross-section of each layer to rotate individually, which increases the accuracy compared to conventional formulations in the literature. The displacement field of the system is presented in a factored matrix form, which is utilized to derive the element mass and stiffness matrices. Theoretical and experimental frequency response functions of a piezopatch and beam system are obtained with the piezopatch electrically open and closed circuited. Better agreement is observed between the presented model and experimental results than is obtained using a Euler–Bernoulli formulation for both layers or Timoshenko theory for only one layer and Euler–Bernoulli theory for the other. The piezoelectric and dielectric behavior of the piezoceramic wafer are included in the element model. An optimized vibration absorber using an electrical resistive-inductive shunt circuit on the piezopatch is also simulated.

1. Introduction

Piezoelectric materials have been proposed for many different engineering applications in the last 15 years [1,2]. Piezopatch actuators are either bonded to the surface or embedded in the host

*Corresponding author. Tel.: +1-312-413-7951.
E-mail address: troyston@uic.edu (T.J. Royston).

0022-460X/$ - see front matter © 2003 Elsevier Ltd. All rights reserved.
doi:10.1016/j.jsv.2003.07.014

structure. Distributed actuators that are embedded in flexible structures have been applied by Bailey and Hubbard [3], Alberts and Colvin [4], Newman [5], and Dimitriadis et al. [6]. Many analytical models have been proposed to predict the interactions between the piezoelectric actuators and host structures. For the dynamic analysis of the system most researchers have assumed that the actuator and substructure were bonded to each other perfectly with a negligible adhesive layer while some have formulated a comprehensive static coupling model, which encompasses the contribution of the elastic bounding layer.

Crawley and de Luis [2] proposed a uniform strain model for a beam with a piezoelectric actuator bonded on the surface. The model also incorporated shear effects of the adhesive layer between the piezoelectric actuator and the beam. Crawley and Anderson [7] developed a Bernoulli–Euler beam model that assumes the entire cross-section of both host structure and actuators undergoes consistent Bernoulli–Euler strains, which can predict both extension and bending modes.

Tylinkowski [8] has proposed a dynamic bending-extension model that includes the bonding layer. Pietrzakowski [9] showed that a model without shear effects could be reasonable only for thin piezoactuators. Benjeddou and Trindale [10] have developed a formulation that can simulate both the extension and shear actuation mechanisms of the beam. In their formulation they have used Euler–Bernoulli theory for piezopatches and Timoshenko beam theory for the thicker core layer.

In most other studies Euler beam theory is adapted to describe kinematic deformation [11–13]. Austin and Inman [14] used a Timoshenko beam model for multilayer sandwich beams (without a piezolayer) that assumed shear stress continuity between the layers. A Ritz–Galerkin approach is used for construction of the mass and stiffness matrices [13,14]. Van Nostrand and Inman [15] developed a finite element approach for the construction of the mass and stiffness matrices. Sung and Kam [16] presented a finite element model for active constrained damping using Mindlin plate theory where only one rotation of cross-section in two directions (on xz and yz planes) was introduced. They also discussed active vibration control via electrical activation of the PZT wafer laminated on the beam. Chattopadhyay and Gu [17] used a hybrid displacement field like the one presented in this paper where the cross-sectional rotation was allowed for individual layers for a plate formulation; however, the piezoelectric effect due to deformation was not identified clearly. Tsai and Wang [18] used an Euler–Beroulli beam for their model and studied characteristics of active piezoactuators that were passively shunted. Abramovich [19] considered a multi-layer beam with laminated piezolayers and considered the rotational cross-section; however, in his model all the layers had the same rotation and the energy dissipation due to the shear among the layers was disregarded.

Based on the literature review, a finite element model (and its experimental validation) using a Timoshenko beam model for a base layer and the piezopatch layer adhered to it is missing. Kusculuoglu et al. [20] recently introduced such a model that treats each individual layer as a Timoshenko beam, yielding more precise results than the Euler–Bernoulli beam model. In the present paper, the piezoelectric and dielectric behavior of the piezopatch layer are incorporated into the model and experimental validation of the model is provided. Additionally, the model is used to optimize and simulate passive vibration control of the piezopatch and beam system via an inductive–resistive "tuned" absorber shunt on the piezopatch.

2. Theory

2.1. Kinematics of deformation

Consider a beam with a piezoceramic patch on it. Fig. 1 shows the deformation of the two layers. Each layer is assumed to deform as a Timoshenko beam. That is, the cross-section normal to the neutral axis before deformation remains plain after deformation but not necessarily perpendicular to the neutral axis.

2.2. Displacement equations

Using Timoshenko beams, the elastic displacement of the aluminum layer is

$$u_1 = u_b - z\psi, \quad u_3 = w. \tag{1}$$

Similarly, the elastic displacement of the piezolayer is

$$u_1 = u_p - z\xi, \quad u_3 = w, \tag{2}$$

where u_1 and u_3 are the elastic displacements along the x- and z- axis, respectively. To ensure the continuity of displacement, u_1 at the interface of aluminum and piezoceramic layer must be equal. That is

$$u_b - \frac{h_b}{2}\psi = u_p + \frac{h_p}{2}\xi. \tag{3}$$

To solve u_p we have

$$u_p = u_b - \frac{h_b}{2}\psi - \frac{h_p}{2}\xi. \tag{4}$$

Hence, the elastic displacement for the piezolayer becomes

$$u_1 = u_b - \frac{h_b}{2}\psi - \left(\frac{h_p}{2} + z\right)\xi, \quad u_3 = w. \tag{5}$$

Eqs. (1) and (5) relate the displacement of an arbitrary point on the base and piezolayers to the elastic displacement of the neutral axis and the rotation of the cross-section.

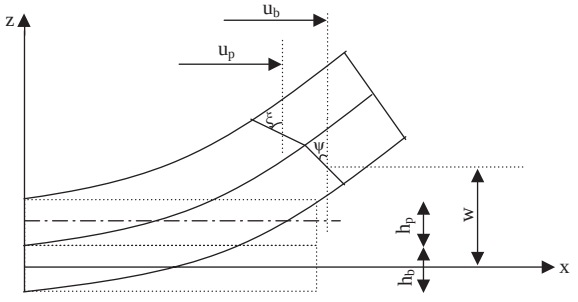

Fig. 1. Schematic of the single beam with piezoelement after deflection.

2.3. Strain equations

Using Eq. (3) we have

$$\begin{bmatrix} u_1 \\ u_3 \end{bmatrix} = S_b \begin{bmatrix} w \\ u_b \\ \psi \\ \xi \end{bmatrix}, \tag{6}$$

where S_b is

$$S_b = \begin{bmatrix} 0 & 1 & -z & 0 \\ 1 & 0 & 0 & 0 \end{bmatrix}. \tag{7}$$

Strains ε_{xx} and ε_{xz} can be defined as

$$\varepsilon_{xx} = \frac{\partial u_1}{\partial x}, \quad 2\varepsilon_{xz} = \frac{\partial u_1}{\partial z} + \frac{\partial u_3}{\partial x}. \tag{8}$$

Substituting Eq. (6) into Eq. (8) yields

$$\begin{bmatrix} \varepsilon_{xx} \\ 2\varepsilon_{xz} \end{bmatrix} = B_b D_b \begin{bmatrix} w \\ u_b \\ \psi \\ \xi \end{bmatrix}, \tag{9}$$

where B_b and D_b are

$$B_b = \begin{bmatrix} 0 & 1 & -z & 0 & 0 & 0 & 0 & 0 \\ 0 & 0 & 0 & 0 & 1 & 0 & -1 & 0 \end{bmatrix}, \quad D_b = \begin{bmatrix} 0 & 0 & 0 & 0 \\ 0 & \dfrac{\partial}{\partial x} & 0 & 0 \\ 0 & 0 & \dfrac{\partial}{\partial x} & 0 \\ 0 & 0 & 0 & 0 \\ \dfrac{\partial}{\partial x} & 0 & 0 & 0 \\ 0 & 0 & 0 & 0 \\ 0 & 0 & 1 & 0 \\ 0 & 0 & 0 & 0 \end{bmatrix}.$$

Similarly, the displacement for the piezolayer in matrix form is

$$\begin{bmatrix} u_1 \\ u_3 \end{bmatrix} = S_p \begin{bmatrix} w \\ u_b \\ \psi \\ \xi \end{bmatrix}, \tag{10}$$

where

$$S_p = \begin{bmatrix} 0 & 1 & -h_b/2 & -(h_p/2+z) \\ 1 & 0 & 0 & 0 \end{bmatrix}.$$

Substituting Eq. (10) into Eq. (8) yields

$$\begin{bmatrix} \varepsilon_{xx} \\ 2\varepsilon_{xz} \end{bmatrix} = B_p D_p \begin{bmatrix} w \\ u_b \\ \psi \\ \xi \end{bmatrix}, \tag{11}$$

where B_p and D_p are

$$B_p = \begin{bmatrix} 0 & 1 & -\dfrac{h_b}{2} & -\left(\dfrac{h_p}{2}+z\right) & 0 & 0 & 0 & 0 \\ 0 & 0 & 0 & 0 & 1 & 0 & 0 & -1 \end{bmatrix}, \quad D_p = \begin{bmatrix} 0 & 0 & 0 & 0 \\ 0 & \dfrac{\partial}{\partial x} & 0 & 0 \\ 0 & 0 & \dfrac{\partial}{\partial x} & 0 \\ 0 & 0 & 0 & \dfrac{\partial}{\partial x} \\ \dfrac{\partial}{\partial x} & 0 & 0 & 0 \\ 0 & 0 & 0 & 0 \\ 0 & 0 & 0 & 0 \\ 0 & 0 & 0 & \dfrac{\partial}{\partial x} \end{bmatrix}.$$

2.4. Element stiffness matrices

Strain energy density of the aluminum and the piezolayers are

$$U_b = \frac{1}{2}[\,\varepsilon_{xx} \quad 2\varepsilon_{xz}\,] \begin{bmatrix} 2G_b(1+\upsilon_b) & 0 \\ 0 & G_b \end{bmatrix} \begin{bmatrix} \varepsilon_{xx} \\ 2\varepsilon_{xz} \end{bmatrix}, \tag{12}$$

$$U_p = \frac{1}{2}[\,\varepsilon_{xx} \quad 2\varepsilon_{xz}\,] \begin{bmatrix} 2G_p(1+\upsilon_p) & 0 \\ 0 & G_p \end{bmatrix} \begin{bmatrix} \varepsilon_{xx} \\ 2\varepsilon_{xz} \end{bmatrix}. \tag{13}$$

Substituting Eqs. (9) and (11) into Eqs. (12) and (13) yields

$$U_b = \frac{1}{2}[\,w \quad u_b \quad \psi \quad \xi\,] D_b^{\mathrm{T}} B_b^{\mathrm{T}} H_b B_b D_b \begin{bmatrix} w \\ u_b \\ \psi \\ \xi \end{bmatrix}, \tag{14}$$

$$U_p = \frac{1}{2}[\, w \quad u_b \quad \psi \quad \xi\,] D_p^{\mathrm{T}} B_p^{\mathrm{T}} H_p B_p D_p \begin{bmatrix} w \\ u_b \\ \psi \\ \xi \end{bmatrix}, \tag{15}$$

where H_a and H_p are

$$H_b = \begin{bmatrix} 2G_b(1+v_b) & 0 \\ 0 & G_b \end{bmatrix}, \quad H_p = \begin{bmatrix} 2G_p(1+v_p) & 0 \\ 0 & G_p \end{bmatrix}.$$

The constitutive relationship between the electrical displacement D (charge/area normal to z), mechanical strain of the piezoceramic (ε), the electric field E (voltage/length in z) and stress is

$$[\,\tau\,] = [\, C_{11}^D \quad -h_{31}\,] \begin{bmatrix} \varepsilon \\ D \end{bmatrix}. \tag{16}$$

Mechanical stress and the potential energy equation for the piezolayer independent of the electric displacement are given in Eq. (16). Coupling terms of the stress with the electrical displacement for the energy expression can be written as

$$E_{p'} = \frac{1}{2}\int_V -h_{31} D\varepsilon \, \mathrm{d}V, \tag{17a}$$

$$E_{p'} = \frac{1}{2}\int_V -h_{31} D\left[\frac{\partial u_b}{\partial x} - \frac{h_b}{2}\frac{\partial \psi}{\partial x} - \left(\frac{h_p}{2} + z\right)\left(\frac{\partial \xi}{\partial x}\right)\right] \mathrm{d}V, \tag{17b}$$

where electric field can be defined as

$$[E] = [\, -g_{31} \quad \beta_{33}^{\mathrm{T}}\,] \begin{bmatrix} \tau \\ D \end{bmatrix}. \tag{18}$$

The potential energy of dielectric effect of the piezolayer can be expressed as

$$E_{pe} = \frac{1}{2}\int_{V_p} (ED)\, \mathrm{d}V. \tag{19}$$

Eq. (19) can be explicitly written as

$$E_{pe} = \frac{1}{2}\int_{V_p} (\beta_{33}^{\mathrm{T}} D^2 + g_{31} h_{31} D^2 - g_{31} C_{11}^D D\varepsilon_{xx})\, \mathrm{d}V. \tag{20}$$

Mechanical strain used in Eq. (20) occurs in the x direction in the piezolayer. Combining Eqs. (8) and (20), the potential energy E_{pe} can be rewritten as

$$E_{pe} = \frac{1}{2}\int_{V_c} \left[\beta_{33}^{\mathrm{T}} D^2 + g_{31} h_{31} D^2 - g_{31} C_{11}^D D\left(\frac{\partial u_c}{\partial x} - z\frac{\partial \xi}{\partial x}\right)\right] \mathrm{d}V. \tag{21}$$

Discretizing the elastic displacements w, u_b, ψ and ξ yields

$$\begin{aligned} &w = N_1 w_i + N_3 w_i' + N_2 w_j + N_4 w_j', \\ &u_a = N_5 u_i + N_6 u_j, \quad \psi = N_5 \psi_i + N_6 \psi_j, \quad \xi = N_5 \xi_i + N_6 \xi_j. \end{aligned} \tag{22}$$

Putting Eq. (24) into matrix form yields

$$[w \quad u_a \quad \psi \quad \xi]^{\mathrm{T}} = Nq, \tag{23}$$

where N and q are

$$N = \begin{bmatrix} N_1 & N_3 & 0 & 0 & 0 & N_2 & N_4 & 0 & 0 & 0 \\ 0 & 0 & N_5 & 0 & 0 & 0 & 0 & N_6 & 0 & 0 \\ 0 & 0 & 0 & N_5 & 0 & 0 & 0 & 0 & N_6 & 0 \\ 0 & 0 & 0 & 0 & N_5 & 0 & 0 & 0 & 0 & N_6 \end{bmatrix},$$

$$q = [w_i \quad w_i' \quad u_{ai} \quad \psi_i \quad \xi_i \quad w_j \quad w_j' \quad u_{aj} \quad \psi_j \quad \xi_j]^{\mathrm{T}}.$$

Here, N_1 through N_6 are shape functions. They are

$$N_1 = 1 - 3\left(\frac{x}{L}\right)^2 + 2\left(\frac{x}{L}\right)^3, \quad N_2 = 3\left(\frac{x}{L}\right)^2 - 2\left(\frac{x}{L}\right)^3, \quad N_3 = -x\left(1 - \frac{x}{L}\right)^2,$$
$$N_4 = -x\left[\left(\frac{x}{L}\right)^2 - \frac{x}{L}\right], \quad N_5 = 1 - \frac{x}{L}, \quad N_6 = \frac{x}{L}.$$

Substituting Eq. (23) into Eqs. (14) and (15) and integrating over the layers yields

$$K_b = \int \left[N^{\mathrm{T}} D_b^{\mathrm{T}} \left[\iint (B_b^{\mathrm{T}} H_b B_b) \, \mathrm{d}y \mathrm{d}z \right] D_b N \right] \mathrm{d}x, \tag{24}$$

$$K_p = \int \left[N^{\mathrm{T}} D_p^{\mathrm{T}} \left[\iint (B_p^{\mathrm{T}} H_p B_p) \, \mathrm{d}y \mathrm{d}z \right] D_p N \right] \mathrm{d}x. \tag{25}$$

Eqs. (24) and (25) suggest that $B_b^{\mathrm{T}} H_b B_b$ and $B_p^{\mathrm{T}} H_p B_p$ should be integrated with respect to y and z first and then the result should be integrated with respect to x. Therefore, the element stiffness matrix becomes

$$K_e = K_b + K_p. \tag{26}$$

Eq. (17) can be discretized as

$$Coup\ H = \int (C_{11}^D g_{31} + h_{31}) A_p S_{pe} D_e N \, \mathrm{d}x. \tag{27}$$

Here, A_p is the area of the piezolayer, and S_p and D_e are

$$S_{pe} = \begin{bmatrix} 0 & -\frac{1}{2} & \frac{h_b}{4} & \frac{h_p}{4} \end{bmatrix}, \quad D_e = \begin{bmatrix} \frac{\partial}{\partial x} & 0 & 0 & 0 \\ 0 & \frac{\partial}{\partial x} & 0 & 0 \\ 0 & 0 & \frac{\partial}{\partial x} & 0 \\ 0 & 0 & 0 & \frac{\partial}{\partial x} \end{bmatrix}.$$

2.5. Element mass matrices

The kinetic energy density for the Timoshenko beam is

$$T = \frac{1}{2}\rho\left(\dot{u}_1^2 + \dot{u}_3^2\right). \tag{28}$$

Therefore, the kinetic energy density of the base and piezolayer become

$$T_b = \frac{1}{2}\rho_b\begin{bmatrix}\dot{u}_1 & \dot{u}_3\end{bmatrix}\begin{bmatrix}\dot{u}_1 \\ \dot{u}_3\end{bmatrix}, \tag{29}$$

$$T_p = \frac{1}{2}\rho_p\begin{bmatrix}\dot{u}_1 & \dot{u}_3\end{bmatrix}\begin{bmatrix}\dot{u}_1 \\ \dot{u}_3\end{bmatrix}. \tag{30}$$

Discretizing Eqs. (6) and (10) using Eq. (17) and then substituting into Eq. (29) and (30) yields

$$T_b = \tfrac{1}{2}\rho_b\dot{q}^{\mathrm{T}}N^{\mathrm{T}}S_b^{\mathrm{T}}S_bN\dot{q}, \tag{31}$$

$$T_p = \tfrac{1}{2}\rho_p\dot{q}^{\mathrm{T}}N^{\mathrm{T}}S_p^{\mathrm{T}}S_pN\dot{q}. \tag{32}$$

Element mass matrices are obtained by integrating Eqs. (31) and (32) over the layers. That is

$$M_b = \rho_b\int\left[N^{\mathrm{T}}\left[\int\int(S_b^{\mathrm{T}}S_b)\,\mathrm{d}y\,\mathrm{d}z\right]N\right]\mathrm{d}x, \tag{33}$$

$$M_p = \rho_p\int\left[N^{\mathrm{T}}\left[\int\int(S_p^{\mathrm{T}}S_p)\,\mathrm{d}y\,\mathrm{d}z\right]N\right]\mathrm{d}x. \tag{34}$$

Therefore, the element mass matrix is

$$M_e = M_b + M_p. \tag{35}$$

Virtual work done by the external disturbance force is

$$\delta W_d = \int_L f(x,t)\,\delta w(x,t)\,\mathrm{d}x. \tag{36}$$

According to the Hamilton's principle one can write

$$\int_{t_1}^{t_2}[\delta T_b + \delta T_p - \delta E_b - \delta E_p - \delta E_{pe} - \delta E_{p'} + \delta W_d]\,\mathrm{d}t = 0. \tag{37}$$

Having derived the element mass and stiffness matrices, they are assembled and used for the differential equation

$$\begin{bmatrix}[M_e] & 0 \\ 0 & L\end{bmatrix}\begin{bmatrix}\ddot{q} \\ \ddot{D}\end{bmatrix} + \begin{bmatrix}[C_e] & 0 \\ 0 & R\end{bmatrix}\begin{bmatrix}\dot{q} \\ \dot{D}\end{bmatrix} + \begin{bmatrix}[K_e] & Coup\ V \\ Coup\ H & 1/C\end{bmatrix}\begin{bmatrix}q \\ D\end{bmatrix} = \begin{bmatrix}Q_e \\ V\end{bmatrix}, \tag{38}$$

where L is inductance and R is the resistor that can be serially connected to the piezolayer. Also, C_e is the damping matrix for the whole system and $Coup\ V$ is a vector that is equal to the

transpose of the row vector *Coup H*. The inverse capacitance term shown as $1/C$ is equal to

$$1/C = h_p\left(g_{31}h_{31} + \beta_{33}^{\mathrm{T}}\right). \tag{39}$$

3. Experiment and simulation results

3.1. Validation of the model—example case #1

To validate the finite element formulation two different beams with different boundary conditions are considered. The first specimen, with material properties given in Table 1, has simply supported boundary conditions. Dimensions of the beam and the orientation of the PZT wafer laminated on the beam are given in Fig. 2. Bonding of the PZT onto the base layer and soldering of the wires were done using Epo-Tek301 epoxy, #30 gage wires, S60 Sn/40Pb solder and Supersafe #67 DSA liquid flux per manufacturer instructions. In the theoretical calculations the bond layer is assumed to be even and thin enough such that its effects can be ignored.

Simply supported (SS) boundary conditions are approximated by using brass shim mounts at either end of the beam that are in turn connected to a rigid fixture. Preventing the vertical displacement of the beam, yet allowing the cross-sectional rotation on each side of the beam, simply supported boundary conditions are satisfied [21,22]. The SS beam is excited by a shaker (Labworks Inc., ET-132-2&203), via an amplifier (Bruel & Kjaer, 2712), and the frequency response is observed using an Agilent (HP) 35670a spectrum analyzer. Excitation of the beam is in the 3 (z) direction and the response in the same direction is measured using an accelerometer (PCB, 309A).

The system, shown in Fig. 3, is first driven in two different configurations: (1) open-circuited resulting in constant D; and (2) close-circuited (with zero inductance and resistance) resulting in

Table 1
Material properties of the base layer and monolithic PZT wafer for example case #1

		Base layer	Piezo layer	Units
Length	L	0.508	0.07239	m
Width	b	0.1016	0.07239	m
Thickness	h	0.00635	0.0002667	m
Density	ρ	2698.5	7800	kg/m^3
Young's modulus	E	6.748×10^{10}	6.2×10^{10}	N/m^2
Piezo-constants	d_{31}	—	-320×10^{-12}	m/V
	d_{33}	—	650×10^{-12}	m/V
	g_{31}	—	-9.5×10^{-3}	Vm/N
	h_{31}	—	-1.35×10^{9}	V/m
Capacitance	C_{pzt}	—	610×10^{-9}	F
Mech. stiffness	C_{11}^{D}	—	13.64×10^{10}	N/m^2
Dielectric constant	β_{33}^{T}	—	4.6808×10^{7}	Vm/C

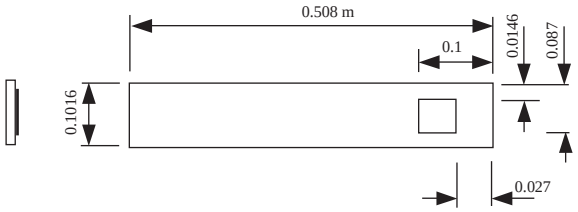

Fig. 2. Dimensions (in meters) of the simply supported beam and piezopatch.

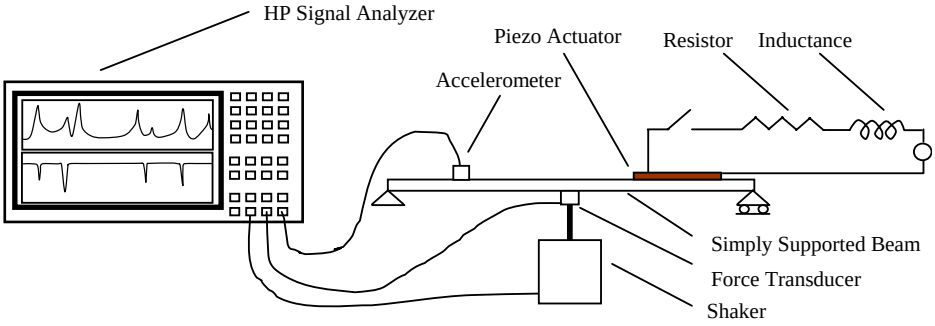

Fig. 3. Experimental setup for the shaker-excited system.

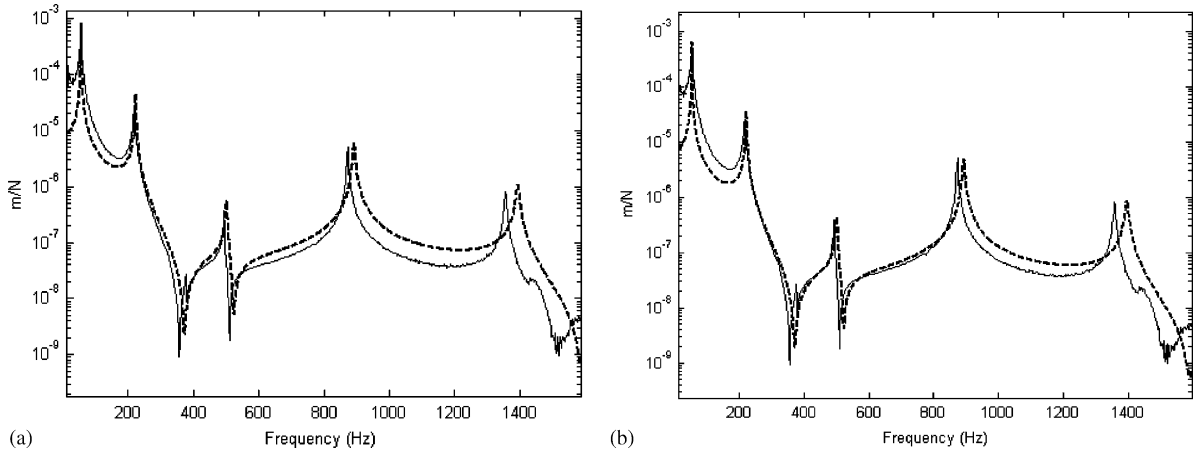

Fig. 4. Experimental and theoretical frequency response (excitation via shaker) of the (a) open circuit system (– – –, proposed FEM; ——, experiment) and (b) closed circuit system (– – –, proposed FEM; ——, experiment).

constant E. In Fig. 4, experimental results and model predictions via FEA with 20 elements are compared for both cases in terms of the frequency response. Mechanical damping is measured experimentally as damping ratios for individual modes using the half-power bandwidth method. The modal damping matrix C_m is formed using the experimental damping ratios; the nodal damping matrix C_e is determined by pre- and post-multiplying C_m with the model matrix of eigenvectors.

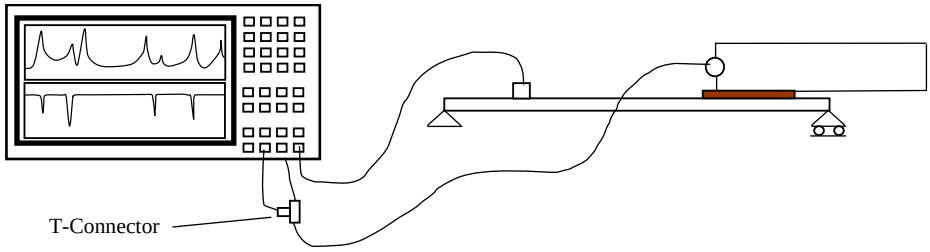

Fig. 5. Experimental setup for the system driven by the PZT wafer.

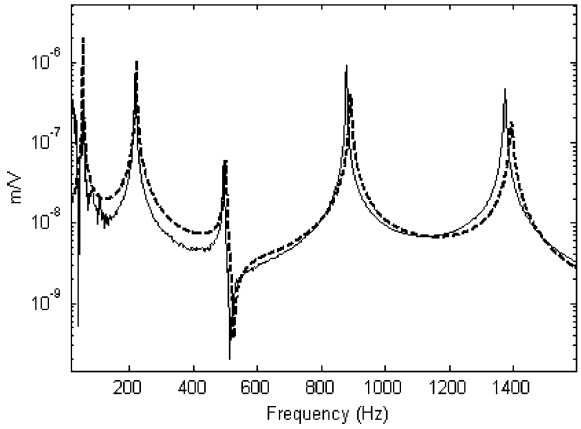

Fig. 6. Experimental and theoretical frequency response of the system driven by the PZT wafer (– – –, proposed FEM; ——, experiment).

Next a broadband random voltage signal is sent to the PZT wafer, itself, as shown in Fig. 5 (without the inductor and resistor). The proposed FE model predictions are compared with experimental results in Fig. 6. Good agreement here, as well as in Fig. 4, suggests that the electrical domain of the piezoelement is also implemented correctly.

It can be argued that the forcing of the system is mainly dominated by the *Coup V* vector and external voltage V, so this simulation cannot fully evaluate the accuracy of the dielectric effect introduced in the FEM formulation. In order to clarify this, an optimization study is done for passive vibration control using a resistive–inductive shunt circuit, which is presented in Section 3.4.

3.2. Advantages of the proposed model

It is proposed that the FE model introduced in this paper provides greater accuracy than previously introduced models by accounting for independent cross-sectional rotation for each layer. To test this hypothesis, comparisons are made with other models for the example case introduced in the previous section. All of the comparisons are presented in Table 2 where natural frequencies are normalized with respect to the first mode of the corresponding method. (The experimentally measured fundamental natural frequency is $f_1 = 55.34$ Hz with all the different

Table 2
Experimental, ANSYS and proposed FEM natural frequencies using 40 divisions along the SS beam (example case #1)

Mode (n)	Exp.	Assumed mode		ANSYS		Single Timoshenko		Proposed FEM	
	f_n/f_1	f_n/f_1	Dev. (%)	f_n/f_1	Dev. (%)	f_n/f_1	Dev. (%)	f_n/f_1	Dev. (%)
1	1.000	1.000	0.0000	1.000	0.0000	1.000	0.0000	1.000	0.0000
2	3.975	3.983	0.0019	4.012	0.0093	3.943	0.0083	3.986	0.0028
3	8.927	9.022	0.0107	9.051	0.0140	8.844	0.0093	8.950	0.0026
4	15.938	16.060	0.0077	16.091	0.0096	15.762	0.0110	15.897	0.0026
5	24.828	24.995	0.0067	25.008	0.0072	24.967	0.0056	24.867	0.0016
6	35.670	36.012	0.0096	35.097	0.0161	37.864	0.0615	35.906	0.0066
7	48.789	49.042	0.0052	49.039	0.0051	49.798	0.0207	49.035	0.0050
8	63.065	64.030	0.0153	65.630	0.0407	64.592	0.0242	64.241	0.0187
9	82.219	81.164	0.0128	82.471	0.0031	85.606	0.0412	81.837	0.0046
10	93.531	100.14	0.0707	101.13	0.0813	102.64	0.0974	93.034	0.0053

methods considered here roughly matching this, within uncertainty limits of the material properties.) In the third column predictions of a normalized assumed mode solution (spectral method) that uses 20 modes are presented, a formulation based on Euler–Bernoulli beam theory. Deviation of the results from the experimental results is reported in the fourth column.

The proposed FE model is also compared to a "single Timoshenko" (conventional FEM) model whose elements have 4-d.o.f. including w, w', u_b and ψ. This model accounts for rotational inertia of the base layer and assumes that the cross-sectional rotation of the PZT layer is identical to the base layer. Unlike the proposed model it does not use an additional d.o.f. for independent rotation of the PZT layer. Table 2 (columns 7–10) compare the FE formulations (all based on 40 elements) with experiment. The proposed FE model more accurately matches experiment as frequency increases.

The proposed FE formulation is also compared with results obtained using the commercial FEA software ANSYS, where the bending natural frequency results are reported in Table 2 (columns 5–6). The coupled field (piezoelectric and mechanical coupling) elements in ANSYS, such as Plane13, Tran109, Solid5 or Solid98 do not have multi layer capability [26]. Thus, in order to make a reasonable comparison a Shell91 element is used for meshing, and simply supported beam boundary conditions are applied with 40 elements along the beam length and 7 elements across its width (280 elements in total) and the fundamental mode is observed at 55.87 Hz. The Shell91 element enforces displacement continuity throughout the layers and uses thin beam theory. An option that comes with the element is called "sandwich option" which enables one of the layer's cross-section to rotate; but, this option can only be used if 3 or more layers exist, which is not applicable to our study since the beam in this example consists of only 2 layers.

The last two columns of Table 2 contain the results obtained with the proposed FE model and the deviation from the experiment. The first natural frequency is predicted at 55.74 Hz using the new FE model, which uses the same meshing configuration as the other two FE solutions discussed above. In Fig. 8 deviation of the normalized approximated solutions from the normalized experimental solution is presented for the same study case in a graphical format. In

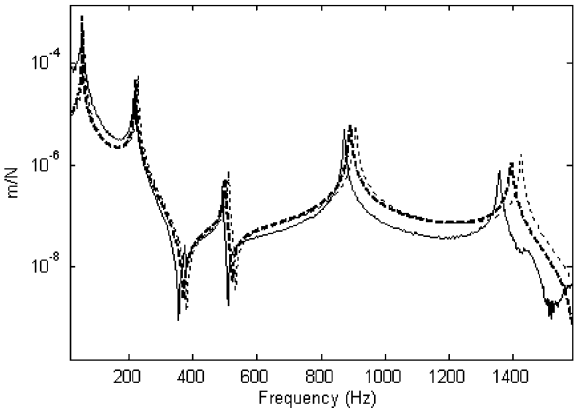

Fig. 7. Experimental, proposed FEM and conventional FEM (single Timoshenko) frequency responses for a closed circuit (constant E) condition (––––, proposed FEM; ----, conventional FEM; ——, experiment).

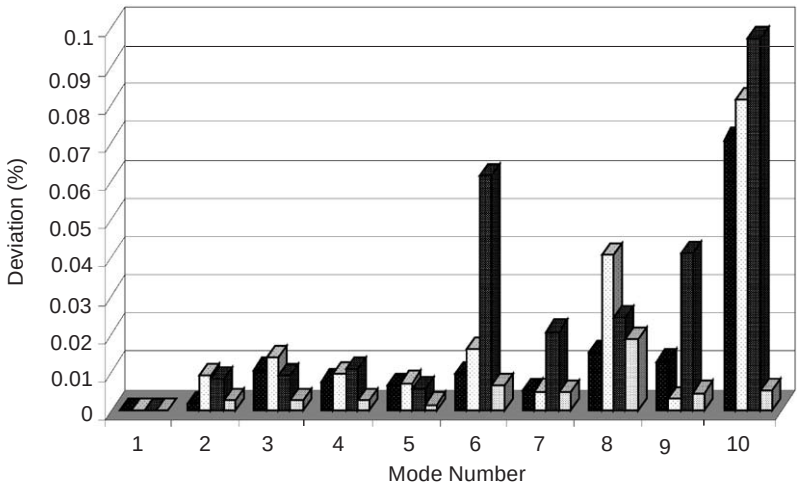

Fig. 8. Deviation of the normalized approximated solutions from normalized experimental solutions for 10 modes. (Columns from left to right consecutively, deviation of assumed mode, ANSYS, single Timoshenko and proposed FEM solution).

this chart deviations of the assumed mode method, ANSYS, single Timoshenko and proposed FE solution are presented by a column for each of the lowest 10 modes. As frequency increases, regardless of the thickness of the structure, inertial forces affect the solution more. This phenomenon can be seen in Fig. 7 where approximated solutions tend to deviate more in the higher modes except for the proposed FEM. Due to the experimental uncertainties the deviation between normalized solutions does not increase linearly with the mode number; however, it can be seen that for almost every single mode the proposed FEM has the minimum deviation. Studying all of the comparisons presented in Table 2, Figs. 7 and 8, it can be seen that the proposed FE model presented in this paper more accurately matches experimental results.

3.3. Advantages of the model in thicker beams—example case #2

In the case studies described above, the improvement in accuracy is not significant as the thickness of the PZT wafer is very small compared to the base layer. Another specimen (Fig. 9) that has a thicker piezolayer, with different boundary conditions, is also studied. This specimen, with dimensions and material properties given in Table 3, has a cantilever (fixed) boundary condition at one end and is free at the other end. The beam is excited via either electrical excitation of the PZT wafer or an impulse hammer and the beam transverse motion is measured using a laser vibrometer. The experimentally measured first natural frequency is 23.4 Hz.

Three different FE solutions and experimental results are presented in Table 4, where all of the natural frequencies are normalized to the fundamental frequency of the corresponding method. All FE solutions use 20 divisions along the beam for meshing (Shell91 elements for ANSYS),

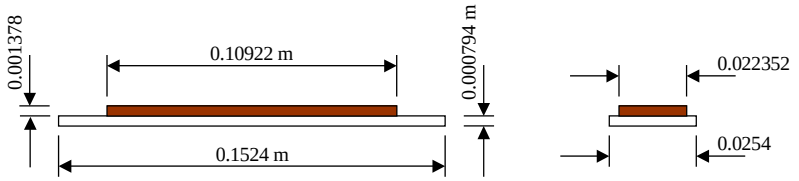

Fig. 9. Dimensions (in meters) for example case #2 with thicker piezoactuator and cantilever boundary conditions.

Table 3
Material properties of example case #2

	Symbol	Base layer	Piezo layer	Units
Length	L	0.1524	0.10922	m
Width	B	0.0254	0.022352	m
Thickness	H	0.000794	0.001378	m
Density	ρ	2799	7800	kg/m^3
Young's modulus	E	7.37739E10	3.1302E10	N/m^2

Table 4
Experimental, ANSYS, single Timoshenko (conventional FEM) and proposed FEM natural frequencies using 20 divisions along the cantilever beam for example case #2

Mode (n)	Experiment	ANSYS		Single Timoshenko		Proposed FEM	
	f_n/f_1	f_n/f_1	Dev. (%)	f_n/f_1	Dev. (%)	f_n/f_1	Dev. (%)
1	1.000	1.000	0.0000	1.000	0.0000	1.000	0.0000
2	11.197	10.702	0.0442	10.952	0.0218	11.197	0.0000
3	32.051	30.039	0.0628	31.775	0.0086	31.974	0.0024
4	54.872	53.725	0.0209	57.577	0.0493	54.924	0.0009
5	85.043	81.686	0.0395	84.448	0.0070	84.932	0.0013
6	129.231	125.490	0.0289	121.984	0.0561	133.701	0.0346
7	209.915	194.471	0.0736	200.099	0.0468	196.265	0.0650

where the first natural frequencies are 24.35, 25.5, and 23.56 Hz for the single Timoshenko (conventional), ANSYS (thin beam) and the proposed FE model, respectively. Here, it can be seen that improvement of the suggested model is more significant than in the results for the first example case study due to the increased piezoceramic thickness.

3.4. Passive control application—extension of example case #1

Most of the papers that can be found in the literature about laminated PZT wafers offer a finite element formulation that can be applicable to active control of a structure. In the formulation given here, the electric charge that is generated in the PZT wafer due to the applied strain is evaluated and used to calculate the overall response of the structure; this enables simulation of electrical passive control capability. In this section, the capability of the proposed FEM to simulate passive control via an electrically shunted PZT is demonstrated. Using the setup depicted in Fig. 3 with the electrical circuit closed, optimized inductance and resistance parameters are evaluated by adapting Den Hartog's [23] well-known method for optimization of damped dynamic vibration absorbers to the PZT-shunt configuration. The frequency response in the vicinity of a specific resonant mode can be targeted for minimization. Using Eq. (38) and assuming that the structural damping sub-matrix C_e is zero the following terms can be defined:

$$\mu = \frac{L}{M}, \quad \omega_a^2 = \frac{1}{LC}, \quad \Omega_n^2 = \frac{K_n}{M_n}, \quad f = \frac{\omega_a}{\Omega_n}, \tag{40a–d}$$

$$g = \frac{\omega}{\Omega_n}, \quad q_{st} = \frac{Q}{K}, \quad R_c = 2L\Omega_n, \quad T = \frac{Coup\ VM\ \ Coup\ HM}{K^2\mu}. \tag{40e–h}$$

Here, M and K are diagonal elements of the modal mass and stiffness matrices, respectively, for the corresponding natural frequency; also, $Coup\ VM$, $Coup\ HM$ and Q are the product matrices of $Coup\ V$, $Coup\ H$, Q_e and the eigenvectors, respectively. The amplitude ratio can be defined as

$$\frac{q}{q_{st}} = \sqrt{\frac{\left(2\frac{R}{R_c}\right)^2 + (g^2 - f^2)^2}{\left(2\frac{R}{R_c}\right)^2 (1^2 - g^2)^2 + [(g^2 - 1)^2(g^2 - f^2)^2 - T^2]}}. \tag{41}$$

The amplitude ratio can be written independent from the resistance value as Ozer and Royston [24,25] have shown. After some algebra optimized inductance and resistance values can be written as

$$L_{opt} = \frac{M}{K}\frac{1}{C}, \quad R_{opt} = \sqrt{\frac{3}{2}\frac{T}{1-(T/2)}}\,\Omega_n \frac{1}{C}. \tag{42a, b}$$

Using the equations defined above the optimum inductance and resistance for the first mode are calculated as 23.7 H and 250 Ω, respectively. Using these values the frequency response is determined for an excitation of 1 N. The force is applied 0.18 m away from the beam end that is further from the PZT wafer and the FE simulation using the proposed method is conducted with 40 elements. The response of the system with and without the LR shunt at node 14 is shown in

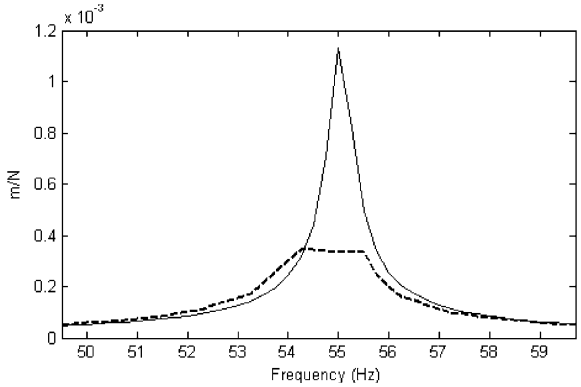

Fig. 10. Frequency response with and without passive control at the first natural frequency for the system of example case #1 (– – – –, optimized LR shunt; ——, no passive control).

Fig. 10. The response of the system at the natural frequency is reduced significantly by the LR shunt under passive conditions.

4. Conclusion

A new finite element model for a beam with a piezoceramic wafer (patch) actuator adhered to it is developed. Each layer is treated as a Timoshenko beam. Constraints are added to ensure the continuity of elastic deformation at the interface. This model is used to generate an expression in factored form for stiffness and mass matrices. These matrices are used in a modal analysis to obtain the natural frequencies. Two experimental studies have validated the theoretical developments. It is also observed that the use of the introduced model becomes more important when the piezoceramic and base layer thickness are large and shear and related rotational inertia become more important. Minor discrepancies observed between the experimental and proposed finite element results are due to experimental uncertainties, and the inherent approximate nature of FE analysis. Also, the system is actively driven by the PZT wafer and a passive control application is studied for the first mode of the system; it is shown that the model is capable of simulating both active and passive control.

Acknowledgements

The research support of the National Science Foundation [Grant #9733565] and the Office of Naval Research [Grant #N00014-99-1-0342] is acknowledged by the first and third authors.

Appendix A. Nomenclature

$u_b(x,t)$ displacement of a point on the neutral axis of the beam along x-axis
$u_p(x,t)$ displacement of a point on the neutral axis of the piezolayer along x-axis
$w(x,t)$ displacement of a point on the neutral axis of the beam

$\psi(x,t)$ rotation of the cross-section of the beam layer
$\xi(x,t)$ rotation of the cross-section of the piezolayer
$u_1(x,t)$ displacement of an arbitrary point along x-axis
$u_3(x,t)$ displacement of an arbitrary point along z-axis
h_b thickness of the beam layer
h_p thickness of the piezolayer
G_a shear modulus of the beam layer
G_p shear modulus of the piezolayer
v_a Poisson ratio of the beam layer
v_p Poisson ratio of the piezolayer
τ mechanical stress (in x direction)
E electric field
D electric displacement
C_{11}^D Young's modulus with open circuit
h_{31} piezoelectric constant
β_{33}^T dielectric constant for piezoactuator
ε mechanical strain for the piezoactuator
A_c cross-sectional area of the piezoactuator
L inductance which is serially connected to the piezoactuator
R resistor which is serially connected to the piezoactuator
C capacitance value of the piezoactuator
V_c control voltage

References

[1] K. Uchino, Electrostrictive actuators: materials and applications, *Ceramic Bulletin* 65 (1986) 647–652.
[2] E. Crawley, J. de Luis, Use of piezoceramic actuators as elements of intelligent structures, *AIAA Journal* 25 (1987) 1373–1385.
[3] T. Bailey, J.E. Hubbard, Distrubted piezoelectric-polymer. Active control of a cantilever beam, *Journal of Guidance Control and Dynamics* 8 (1985) 605–611.
[4] T.E. Alberts, J.A. Colvin, Transfer function analysis for a flexible beam with piezo electric film actuator and sensor, *Proceedings of the Conference on Recent Advantages in Active Control of Sound and Vibration*, Virginia, 1991, pp. 67–77.
[5] M.J. Newman, Distributed active vibration controllers, *Proceedings of the Conference on Recent Advantages in Active Control of Sound and Vibration*, Virginia, 1991, pp. 579–592.
[6] E. Dimitriadis, C.R. Fuller, C.A. Rogers, Piezoelectric actuators for distributed vibration excitation of thin plates, *Journal of Applied Mechanics* 113 (1991) 100–107.
[7] E. Crawley, E. Anderson, Detailed models of piezoelectric actuation of beams, *Proceedings of the 30th AIAA/ASME/SAE Structures, Structural Dynamics, and Material Conference*, Washington, DC, April 1989, pp. 2000–2010.
[8] A. Tylinkowski, Stabilization of beam parametric vibrations, *Journal of Theoretical and Applied Mechanics* 31 (1993) 657–670.
[9] M. Pietrzakowski, Multiple piezoceramic segments in structural vibration control, *Journal of Theoretical and Applied Mechanics* 38 (2000) 35–50.
[10] A. Benjeddou, M.A. Trindale, Piezoelectric active vibration control of damped sandwich beams, *Journal of Vibration and Acoustics* 246 (2001) 653–677.

[11] J.A. Rongong, J.R. Wright, R.J. Wynne, G.R. Tomlinson, Modeling of a hybrid constrained layer/piezoceramic approach to active damping, *Journal of Vibration and Acoustics* 119 (1997) 120–130.
[12] Y. Liu, K.W. Wang, Active passive constrained layer for structural 2damping augmentation, *Journal of Vibration and Acoustics* 122 (2000) 254–262.
[13] J.M. Lam, D.J. Inman, W.R. Saunders, Vibration control through passive constrained damping and active control, *Journal of Intelligent Material Systems and Structures* 8 (1997) 663–677.
[14] E.M. Austin, D.J. Inman, Studies on the kinematic assumptions for sandwich beams, *SPIE* 3045 (1997) 173–183.
[15] W. Van Nostrand, D.J. Inman, Finite element model for active constrained layer damping, *SPIE* 2427 (1995) 124–139.
[16] Y. Sung, Y.S. Kam, A finite element formulation for composite laminates with smart constrained layer damping, *Advances in Engineering Software* 31 (8–9) (2000) 529–537.
[17] A. Chattopadhyay, H.Z. Gu, R. Beri, C.H. Nam, Modeling segmented active constrained layer damping using hybrid displacement field, *AIAA Journal* 39 (3) (2001) 480–486.
[18] M.S. Tsai, K.W. Wang, On the structural damping characteristics of active piezoelectric actuators with passive shunt, *Journal of Sound and Vibration* 221 (1) (1999) 1–22.
[19] H. Abramovich, Deflection control of laminated composite beams with piezoceramic layers - closed form solutions, *Composite Structures* 43 (3) (1998) 217–231.
[20] Z.K. Kusculuoglu, B. Fallahi, T.J. Royston, New constitutive model for vibrations of beam with a piezoceramic patch actuator, *SPIE* 4693 (2002) 92–103.
[21] H. Jiaqiang Pan, Colin, Hansen, Active control of power flow from a vibrating rigid body to a flexible panel through two active isolators, *Journal of the American Statistical Association* 93 (4) (1993) 1947–1953.
[22] H. Jiaqiang Pan, Colin, Hansen, Jie Pan, Active isolation of a vibration source from a thin beam using a single active mount, *Journal of the American Statistical Association* 94 (3) (1993) 1425–1434.
[23] J.P. Den Hartog, *Mechanical Vibrations*, Dover Publications Inc., New York, 1985, pp. 93–104.
[24] M.B. Ozer, T.J. Royston, Optimal passive and hybrid control of vibration and sound radiation from linear and nonlinear PZT-based smart structures, *SPIE* 4693 (2002) 69–80.
[25] M.B. Ozer, T.J. Royston, Passively minimizing structural sound radiation using shunted piezoelectric materials, *Journal of the Acoustical Society of America* 114 (4) (2003) 1934–1946.
[26] ANSYS 6.1, User Manual, ANSYS, Inc. Canonsburg, PA, 2002.